Pore Pressure Prediction in Offshore Niger Delta: Implications on Drilling and Reservoir Quality

Joshua Pwavodi[1], Ibekwe N Kelechi[2], Perekebina Angalabiri[1], Sharon Emeremgini[3], and Oguadinma O Vivian[4]

[1]Univ. Grenoble Alpes
[2]TotalEnergies SA CSTJF
[3]University of Benin
[4]Univ. Lille

November 23, 2022

Abstract

Despite exploration and production success in Niger Delta, several failed wells have been encountered due to overpressures. Hence, it is very essential to understand the spatial distribution of pore pressure and the generating mechanism in order to mitigate the pitfalls that might arise during drilling. This research provides estimates of pore pressure along three offshore wells using the Eaton's transit time method. An accurate normal compaction trend was estimated using the Eaton's exponent (m=3). Our results show that there are three pressure magnitude regimes: normal pressure zone (hydrostatic pressure), Transition pressure zone (slightly above hydrostatic pressure), and over pressured zone (significantly above hydrostatic pressure). The top of the geopressured zone (2873 mbRT or 9425.853 ft) averagely marks the onset of overpressurization with the excess pore pressure ratios above hydrostatic pressure varying averagely along the three wells between P * = 1.06 - 24.75 MPa and the lithostatic load range is λ = 0.46 - 0.97 and λ * = 0.2 - 0.9. The parametric study shows that the value of Eaton's exponent (m = 3-6) need to be applied with caution based on the dominant pore pressure generating mechanism in the Niger Delta. The generating mechanisms responsible for high pore pressure in the Offshore Niger Delta are disequilibrium compaction, unloading (fluid expansion) and shale diagenesis.

Pore Pressure Prediction in Offshore Niger Delta: Implications on Drilling and Reservoir Quality

Pwavodi Joshua[1], Ibekwe N. Kelechi[3], Perekebina Angalabiri[1], Emeremgini Sharon Chioma [4], Oguadinma O. Vivian[2,3]

[1]Univ. Grenoble Alpes, Univ. Savoie Mont Blanc, CNRS, IRD, UGE, ISTerre, 38000 Grenoble, France
[2]Univ. Lille, CNRS, Univ. Littoral Cote d'Opale, UMR 8187, LOG, Laboratoire d'Oceanologie et de Geosciences, 59000, Lille, France
[3]TotalEnergies SA CSTJF, Avenue Larribau, 64000 Pau, France
[4]Centre of Excellence in Petroleum Geoscience and Engineering, University of Benin, Benin City, Edo State

Corresponding author: Joshua Pwavodi, `joshua.pwavodi@univ-grenoble-alpes.fr`

Abstract

Despite exploration and production success in Niger Delta, several failed wells have been encountered due to overpressures. Hence, it is very essential to understand the spatial distribution of pore pressure and the generating mechanism in order to mitigate the pitfalls that might arise during drilling. This research provides estimates of pore pressure along three offshore wells using the Eaton's transit time method. An accurate normal compaction trend was estimated using the Eaton's exponent (m=3). Our results show that there are three pressure magnitude regimes: normal pressure zone (hydrostatic pressure), Transition pressure zone (slightly above hydrostatic pressure), and over pressured zone (significantly above hydrostatic pressure). The top of the geopressured zone (2873 mbRT or 9425.853 ft) averagely marks the onset of overpressurization with the excess pore pressure ratios above hydrostatic pressure varying averagely along the three wells between $P^* = 1.06 - 24.75$ MPa and the lithostatic load range is $\lambda = 0.46 - 0.97$ and $\lambda^* = 0.2 - 0.9$. The parametric study shows that the value of Eaton's exponent (m = 3-6) need to be applied with caution based on the dominant pore pressure generating mechanism in the Niger Delta. The generating mechanisms responsible for high pore pressure in the Offshore Niger Delta are disequilibrium compaction, unloading (fluid expansion) and shale diagenesis.

Keyword: Niger Delta, Pore pressure, Reservoir, Drilling, Fracture pressure, Well logs, Sediments compaction.

1 Introduction

Serious drilling incidents such as kicks & blowouts and other well-related complexities are largely influenced by high pore pressures (Skalle & Podio, 1998; Holand, 2001; J. Zhang, 2011; J. Zhang & Yin, 2017; Baouche et al., 2020; Ganguli & Sen, 2020). Therefore successful drilling campaigns are achieved when the pore pressure regime within an oil basin or other geological settings is properly understood (Pwavodi & Doan, 2022). Several methods have been used to understand and characterised the pore pressure regime in the Niger Delta, yet several drilling incidences (Opara et al., 2009; Nwaufa W.A., 2006; Asedegbega et al., 2018) and overpressures have been identified within this hydrocarbon basin (Dosunmu, 2002; Opara et al., 2013; Ugwu & Nwankwo, 2014; Ichara & Avbovbo, 1985; Opara et al., 2009; Nwaufa W.A., 2006; Alabere & Akangbe, 2021).

Previous studies carried out in the Niger Delta have shown that abnormal pore fluid pressure generation is related to several factors: due to disequilibrium compaction (Ichara & Avbovbo, 1985; Weber & Daukoru, 1975; Nwankwo & Kalu, 2016; Adewole et al., 2016; Udo et al., 2020; Abijah & Tse, 2016; Emudianughe & Ogagarue, 2019; Alabere & Akangbe, 2021), stratigraphic and structural controls (Evamy et al., 1978; Opara et al., 2009; Ugwu & Nwankwo, 2014) and due to normal faulting, clay diapirism, Shale diagenesis and late hydrocarbon generation (Ugwu & Nwankwo, 2014; Opara et al., 2009; Evamy et al., 1978; Nwaufa W.A., 2006; Alabere & Akangbe, 2021). These studies used well logs, seismic data and leak-off test (LOT) to predict pore pressures in the Niger Delta.

Despite inputs from previous studies about the state of pore pressure in the Niger Delta, several failed wells have been encountered and abandoned due to undetected high pore pressures (Opara et al., 2009; Nwaufa W.A., 2006). Hence, suggesting that these methods have not properly predicted the spatial variation of high pore pressure along borehole length in the Niger Delta. The problem mainly stems from poor prediction and understanding of the normal compaction trend (NCT) of sediments in the Niger Delta. Thus, underestimating the actual consolidation history of sediments. Pwavodi and Doan (2022) showed that the normal compaction trend is affected by structural control and fluid flow within a geological setting. Therefore the reliability of pore pressure prediction depends on the accurate estimation of the NCT of the sediments.

In this study, we estimated the spatial variation of pore pressure at a metric scale along 3 boreholes using Eaton's transit time method. Sonic log data was used as a key input to carefully provide accurate normal compaction trend in the study area. The originality of our studies uses python programming for data processing, visualization and pore pressure prediction. It is advantageous using python programming because it gives the flexibility for data manipulation and implementation of Eaton's equation; unlike other studies that used blackbox softwares, which limits their ability to process the data and implement the methodology accurately. This work is the first to provide insights into the lithostatic load and excess pore pressure information in the Niger Delta Basin.

2 Geology of Niger Delta

The study area is located in the Offshore Niger Delta (Figure 1a, b), which has been described as a complex geological environment resulting from deep-seated shale deformation, shale diapirism, and faulting (Tuttle et al., 1999). The Niger Delta Basin is the youngest and most southern sub-basin located at the southwestern boundary in the Benue-Abakaliki trough (Tuttle et al., 1999). It is characterised as a wave-dominated delta located on the Gulf of Guinea continental margin that is formed in the Paleogene with a maximum thickness of about 12km and $75000km^2$ in size (Whiteman, 1982; Haack et al., 2000). The delta has prograded seaward, forming several depositional centres called depobelts (Figure 1b) (Doust H, 1990).

Niger Delta is divided into three broad formations (Akata, Agbada and Benin) (Figure 1c), representing prograding depositional facies that are distinguished mostly based on sand-shale ratio (Avbovbo, 1978). Akata Formation forms the base of the delta (Figure 1c). It is characterised by dark grey marine shale, deposited in the deep sea characterized by low energy condition and oxygen deficiency (Doust H, 1990; Michele L. Tuttle & Brownfield, 1999). Agbada Formation consists of paralic clastics of over 3.7km thick at the central part (Figure 1c), and represents a coarsening upward regressive sequence of sandstone and shale of the delta front, distributary channel and delta plain (Reijers et al., 1997). Benin Formation is the uppermost sedimentary sequence of the basin (Figure 1c), and it is composed of continental sands of alluvial coastal plain origin with local thin shale inter-beds considered to be of braided stream origin (Short & Stauble, 1967; Owoyemi & Willis, 2006; Omoboriowo & Chiadikobi, 2012). The structural complexities of the Niger Delta (Figure 1c) have been identified as depositional belts with distinct structural styles (Ejedawe et al., 1984; Ejedawe, 1989; Knox & Omatsola, 1989). The major syn-sedimentary faults identified in the depobelts include growth faults, crestal faults, counter-regional faults, and antithetic faults (Doust H, 1990; Evamy et al., 1978).

3 Methodology

The methodology used in this work provides consistent results derived from Eaton's equation from three boreholes, $well-05$, $well-10$ and $well-12$ (Figure 2) located in the Offshore Niger Delta (Figure 1a, b). Detailed data processing steps were adopted before the full implementation of the pore pressure prediction. The results from all the wells were compared to understand the spatial distribution of pore pressure within the oil field. The list of notation and symbols used in this research work is given in Table 2.

3.1 Data QC and Processing

Detailed data exploration and processing were carried out to ensure that all unwanted data points (including; negative data points and positive outliers) that could increase the percentage error bar were cleaned. Rolling mean average was used to reduce data randomness in this research. Two preliminary corrections were made on the data. (1) Data cleaning: The datasets were loaded into python jupyter scripts as LAS extension files and presented

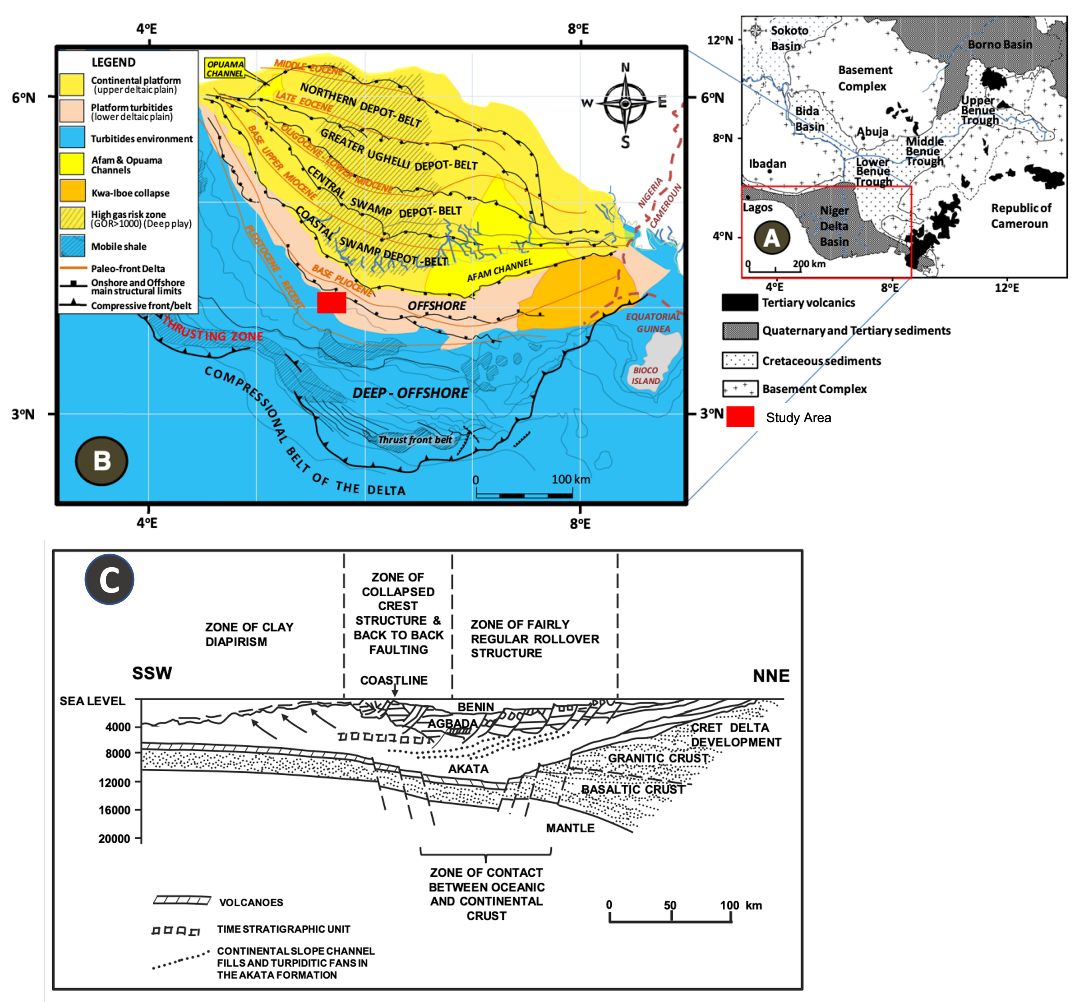

Figure 1. (a & b)Map of the Niger Delta Basin showing the location of study highlighted in red box, with a detailed sectional map of depobelts and structural limits of Niger Delta (modified from Ebong et al. (2020); Doust H (1990)), (c) The stratigraphic succession of the Niger Delta (modified from Whiteman (1982)

in readable formats as DataFrames. Missing data points (Null of NaNs) are replaced with either the mean values, preceding or succeeding data points; assuming the spread of the data points is similar due to close depth interval or same lithology. Outliers are completely removed, or a rolling mean average is used to have reasonable statistical distribution.

(2) Accounting the depth of the seawater column: The initial depths are measured from the rotary table (meters below the rotary table (mbRT)) in the drilling platform as the reference point (Figure 2). In order to obtain the new borehole measured depth (MD) with the seafloor (mudline) depth as a reference level (meters below the seafloor). The seawater column was subtracted from the TD (total depths) in mbRT ($MD[mbsf] = TD[mbRT] - Z_w[m]$) (Table 1). This is important because it helps to determine the exact pressure of the seafloor ($P_{sea} = \rho_w Z_w g$) where, P_{sea} is the pressure at the mudline, ρ_w is the density of the seawater, Z_w is the seawater column, and g is the acceleration due to gravity.

Table 1. The different depth type and seafloor pressure for the three wells location.

Hole	Total borehole length (mbRT)	Seafloor Depth (m)	Borehole length (mbsf)	Seafloor Pressure (Pa)
Well-05	4409.80	1928.28	2481.52	19446086.75
Well-10	4509.80	2005	2504.80	20219783.4
Well-12	4504.943	1659.6	2639.80	16736534.92

Table 2. symbols and notation

Acronym or Symbol	Meaning
P_{sea}	Seawater Pressure at the seafloor
ϕ	Porosity
Z	True Vertical Depth (TVD)
ρ_g	Density of the rock matrix (=grain density)
ρ_r	Rock formation density
ρ_w	Density of the fluid
P_f	Pore fluid pressure
P_{pg}	Pore pressure gradient
σv	Total overburden stress
σv_g	Overburden gradient
P_{hg}	Hydrostatic pressure gradient
P_h	Hydrostatic pressure
σ_e	Effective stress
m	Cementation exponent
Δt	shale transit time from well log
Δt_n	shale transit time in normal pressure condition
Δt_m	shale matrix transit time
Δt_{ml}	Transit time at the mudline ($Z = 0$)
c	Compaction parameter
v	Poisson ratio
V_p	Sonic velocity
V_s	Shear velocity
P_{frac}	Fracture pressure gradient

3.2 Pore Pressure Modelling Using Sonic Travel Time

Pore pressure conditions are controlled by the rock's fluid retention capacity, permeability, under-compaction, loading history or tectonics (Davis et al., 1983; Rubey & King Hubbert, 1959; Tobin & Kinoshita, 2007). In a simple drained diagenetic process the compaction, evolution of these sediments supports an increase in vertical overburden stress (Terzaghi et al., 1968). Sediment compact is considered normal compaction trend (NCT) under hydrostatic pressure. Pore pressure below hydrostatic is called underpressure while above hydrostatic pressure is termed overpressured).

Anomalous pore pressures can result when there is partial expulsion of fluid from pores due to rapid sediment subsidence and low permeability condition (J. J. Zhang, 2019). The remaining fluid in the pores will support all or part of the weight of the overburden sediments resulting in less pore compaction and high porosity scenario (J. J. Zhang, 2019). This leads to high fluid pressure due to compaction disequilibrium or undercompaction. Terzaghi and Peck (1948) proposed a relationship for estimating pore pressure: Terzaghi and Peck (1948):

$$\sigma v \;=\; \sigma_e + P_f \tag{1}$$

Where, P_f is the the pore pressure, σv is the total overburden stress, σ_e is the effective stress.

3.2.1 *Overburden Pressure*

Overburden stress or vertical stress (σv) at a given depth is the total exerted pressure on a formation by the total weight of the overlying rocks and fluids above. The overburden stress was estimated using bulk density log data in well-10 and well-12, while in well-05 the bulk density was derived from the porosity and grain density using:

$$\rho_b = \phi\rho_w + (1-\phi)\rho_r \tag{2}$$

Where ρ_b is the bulk density, ϕ is the porosity, ρ_w is the density of water and ρ_r is the density of the matrix.

The overburden pressure is estimated by integrating the bulk density from the seafloor, considering seafloor pressure and the true vertical depth. The overburden gradient (σv_g) can be estimated using the equation below:

$$\sigma v_g \;=\; \frac{\left(P_{sea} + \int_0^Z \rho_b(Z)\, g\, dZ\right) - P_{sea}}{Z} = \frac{\int_0^Z \rho_b(Z)\, dZ}{Z}\, g \tag{3}$$

3.2.2 *Hydrostatic Pressure*

This is the fluid pressure exerted at a given depth within the fluid, due to gravitational force. This pressure increases with depth from the seafloor due to the increase in the weight of the fluid that exerts downward force from the top. Hydrostatic pressure gradient (P_{hg}) is calculated using the equation below:

$$P_{hg} \;=\; \frac{(P_{sea} + \rho_w\, g\, Z) - P_{sea}}{Z} = \rho_w\, g \tag{4}$$

3.2.3 *Pore Pressure*

Eaton's empirical technique (Eaton, 1972, 1975) establishes a relationship between the pressure gradient, drilling & electrical well log, and the NCT. In drilling, pressure gradients are more convenient when determining the mud weight (J. J. Zhang, 2019). Due

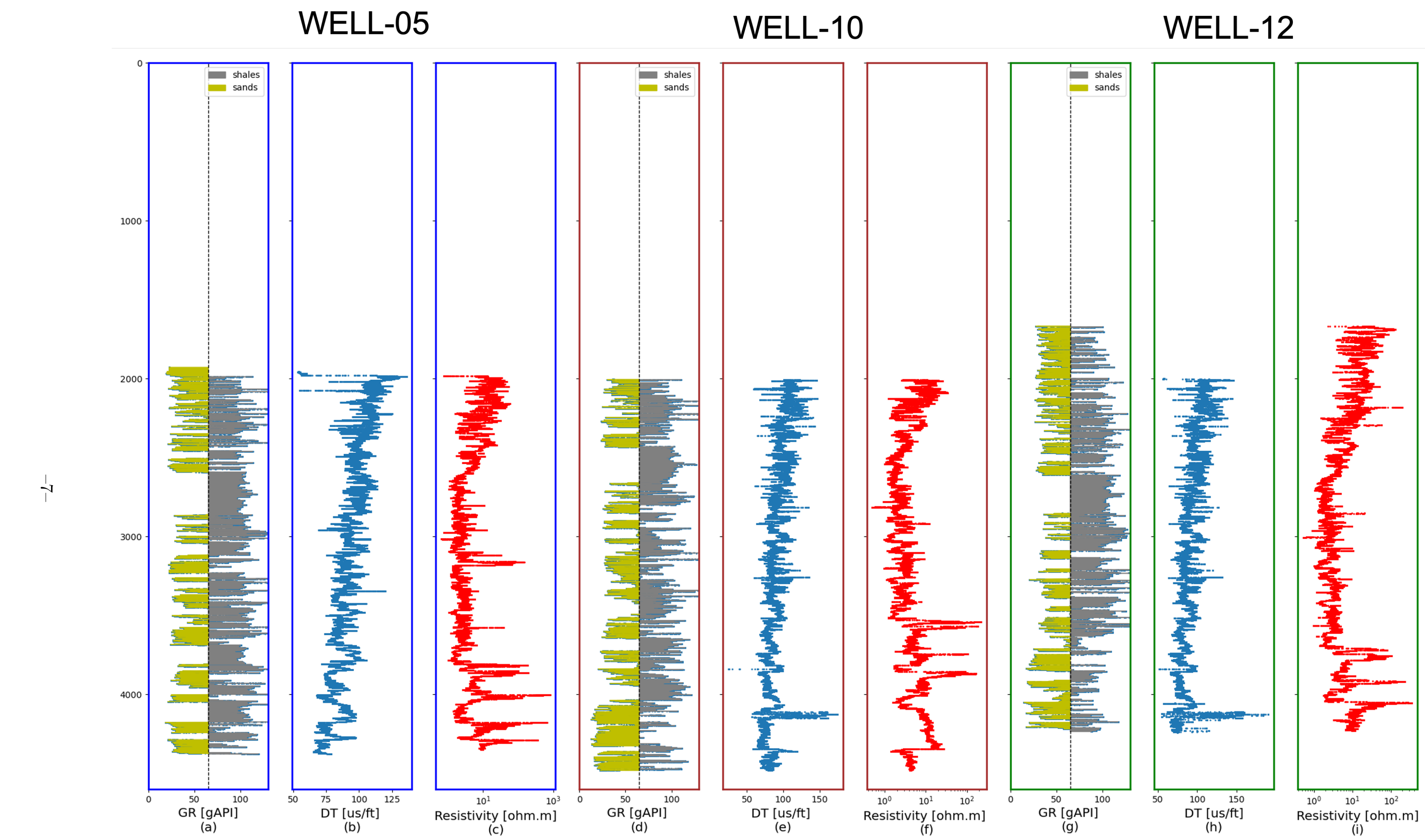

Figure 2. Summary of the geophysical data of Well-05 (a) Natural gamma ray log (GR, API units) (b) Sonic slowness (δt, in μs/ft) (c) Deep electrical resistivity log in $\Omega \cdot$ m. Summary of the geophysical data of Well-10, Well-12 in mbRT (d) Natural gamma ray log (GR, API units) (e) Sonic slowness (δt, in μs/ft) (f) Deep electrical resistivity log in $\Omega \cdot$ m. Summary of the geophysical data of Well-10, Well-12 in mbRT (g) Natural gamma ray log (GR, API units) (h) Sonic slowness (δt, in μs/ft) (i) Deep electrical resistivity log in $\Omega \cdot$ m.

to unavailable broad spectrum of data such as drilling parameters, only the sonic transit time (Eaton, 1975) Eaton's method is used. Pore pressure is estimated using the equation below:

$$P_{pg} = \sigma v_g - (\sigma v_g - P_{hg}) \left(\frac{\Delta t_n}{\Delta t} \right)^m \tag{5}$$

Where, Δt is shale transit time from well log, Δt_n is the transit time in shales (normal pressure condition), and m is an exponent (empirically, m=3).

The departure of the sonic slowness away from the NCT to higher values indicates evidence of overpressure if it is within the same lithology. The NCT was estimated by fitting an exponential relationship between sonic travel time with drilled depth:

$$\Delta t_n = \Delta t_m - (\Delta t_{ml} - \Delta t_m)\ e^{-cz} \tag{6}$$

$$P_f \quad = \quad P_{sea} + P_{pg} Z \tag{7}$$

Where Δt_m is the shale matrix transit time, Δt_{ml} is the mudline transit time ($Z = 0$), Z is the true vertical depth below the mudline (mbsf), and c is the compaction parameter. The pore pressure is estimated using Equation 7. Trend deviations of Δt relative to NCT are clear indications of abnormal pressure zones.

The results of pore pressure is expressed based on Yaolin Shi and Chi-Yuen Wang (1988) as excess pore pressure above hydrostatic pressures:

$$P^* = P_f - P_h \tag{8}$$

The lithostatic load is expressed as an overpressure ratio (Rubey & King Hubbert, 1959):

$$\lambda = \frac{P_f}{\sigma_v} \tag{9}$$

The modified excess pore pressure ratio is expressed as in (Davis et al., 1983):

$$\lambda^* = \frac{(P_f - P_h)}{(\sigma_v - P_h)} \tag{10}$$

Excess pore pressure (P^*) is normalized in relation to the lithostatic pressure with λ^*=0 (hydrostatic pressure), and λ^*=1 (lithostatic pressure).

3.2.4 Fracture Pressure

This is the pressure above which the formation hydraulically fractures (Hubbert et al., 1957; J. Zhang & Yin, 2017). The risk associated with drilling and wellbore stability can be greatly reduced by estimating the fracture gradient. Hubbert et al. (1957) showed that fracture pressure is a function of overburden stress, pore pressure and the Poisson ratio of rocks:

$$P_{frac} = \frac{v}{1-v}(\sigma_v - P_f) + P_f \tag{11}$$

Where; v is the Poisson ratio (dimensionless),

3.2.5 Poisson's Ratio

Poisson ratio can be used to determine the percentage of loose connections in a sediment package (Gercek, 2007). It is a rock's elastic constant which is the inverse of the ratio of axial to transverse strain in an elastic material under a uniaxial stress (Gercek, 2007). Poisson ratio is obtained from the compressional and shear waves (Imhanzuaria & Bello, 2019):

$$v = \frac{v_p^2 - v_s^2}{2(v_p^2 - v_s^2)} \tag{12}$$

Where; v_p is the primary wave velocity (m/s), and v_s is the shear velocity (m/s).

4 Results

4.1 Pore Pressure Results

Pore pressure results are classified into three pressure regimes (normal pressure zone, transitional pressure zone and overpressure zone) with respect to borehole length of the three wells (Well-05, Well-10 & Well-12).

4.1.1 Pore Pressure Along Well-05

Transit time (Δt) follows the NCT (Figure 3c) between the depth range of 0 to 670 mbsf. Generally, the pore pressure gradient is about 1.0 g/cm^3 (Figure 3d) in this interval. Therefore, the pore pressure is equal to the hydrostatic pore pressure (Figure 3e). Hence, it is considered to be normally pressure or hydrostatically pressure.

Trend deviations are observed between 670 mbsf to 1110 mbsf with pore pressure gradient rising to about 1.42 g/cm^3 (Figure 3d). At this depth the formations are already getting pressurized with increasing pore fluid pressure values higher than the hydrostatic pore pressure (Figure 3e). The excess pore pressure above the hydrostatic pressure ranges between $P^* \approx 0.79 - 2.52$ MPa, while, the lithostatic load and modified excess pore pressure ranges between ($\lambda \approx 0.7 - 0.9$) and ($\lambda^* \approx 0.14 - 0.43$) respectively. This interval is considered to be the transitional pore pressure zone.

The bottom of the transitional zone marks the top of the geopressured interval (Figure 3e). Varying trend deviation is consistently observed from the top of the geopressured zone to the bottom of the well (Figure 3 c). In general, the pore pressure gradient rises to a maximum value of 1.58 g/cm^3 (Figure 3d) and alternates back to 1.0 g/cm^3 and to lower values at the bottom of the well. In this interval, the pore pressure consistently increases to values higher than the hydrostatic pressure (Figure 3e). Pore pressure values rises to a maximum value of 52.61 MPa (Figure 3e) but at the bottom of the borehole, intervals with high resistivity signature values (Figure 3b) are hydrostatically pressured or underpressured (Figure 3 e). The excess pore pressure above the hydrostatic pressure ranges between $P^* \approx 1.06 - 12.96$ MPa, while, the lithostatic load and modified excess pore pressure ranges between ($\lambda \approx 0.63 - 0.87$) and ($\lambda^* \approx 0.1 - 0.59$) respectively.

4.1.2 Pore Pressure along Well-10

Transit time (Δt) follows the NCT (Figure 4c) between the depth range of 0 to 457 mbsf. Generally, the pore pressure gradient is about 1.0 g/cm^3 (Figure 4d) in this interval. Therefore, the pore pressure is equal to the hydrostatic pore pressure (Figure 4e). Hence, it is considered to be normally pressure or hydrostatically pressure.

Trend deviations are observed between 457 mbsf to 868 mbsf with pore pressure gradient rising to about 1.42 g/cm^3 (Figure 4d). At this depth the formations are already getting pressurized with increasing pore fluid pressure values higher than the hydrostatic pore pressure (Figure 4e). The excess pore pressure above the hydrostatic pressure ranges between $P^* \approx 0.87 - 2.2$ MPa, while, the lithostatic load and modified excess pore pressure ranges between ($\lambda \approx 0.7 - 0.9$) and ($\lambda^* \approx 0.1 - 0.33$) respectively. This interval is considered to be the transitional pore pressure zone.

The bottom of the transitional zone marks the top of the geopressured interval (Figure 4e). Varying trend deviation is consistently observed from the top of the geopressured zone to the bottom of the well (Figure 4 c). In general, the pore pressure gradient rises to a maximum value of 1.58 g/cm^3 (Figure 4d) and alternates back to 1.0 g/cm^3 and to lower values at the bottom of the well. In this interval, the pore pressure consistently increases to values higher than the hydrostatic pressure (Figure 4e). Pore pressure values rises to a maximum value of 68.59 MPa (Figure 4e) but at the bottom of the borehole, intervals with

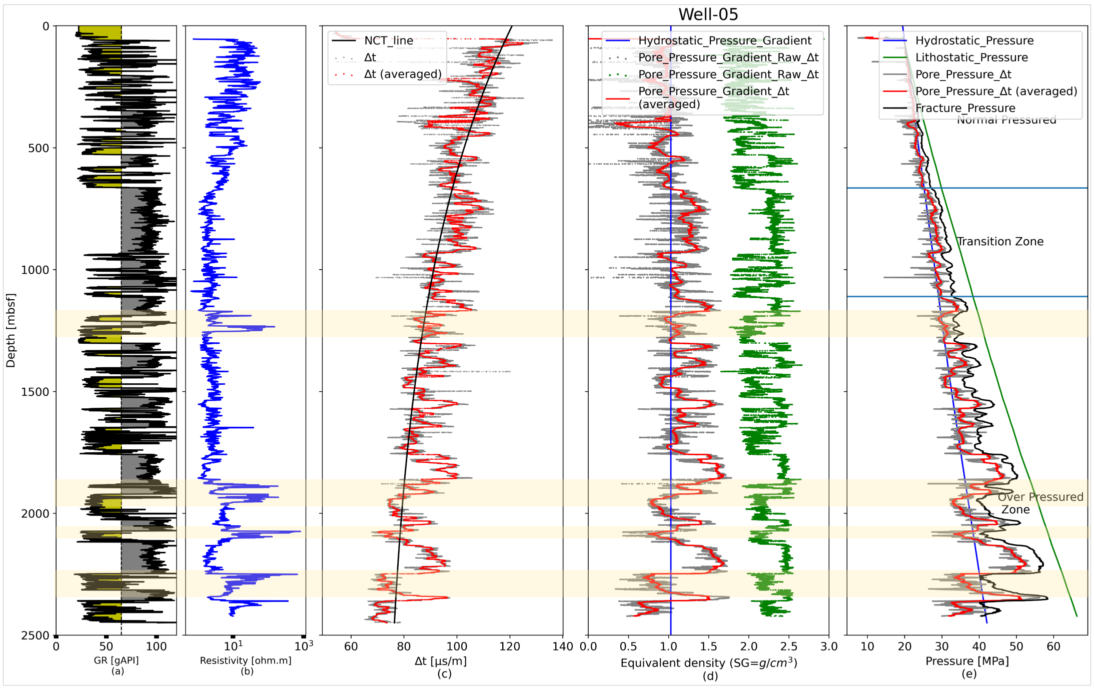

Figure 3. Pore pressure prediction from Eaton modelling based on Δt sonic method (a) Logging units (b) Deep electrical resistivity log in $\Omega \cdot$ m (c)Eaton Δt coefficient profile (raw Δt [gray] and sampled Δt [in red]) and NCT line [in black]. (d) Gradient plots: Pressure gradient pressure gradients, the hydrostatic pressure gradient [blue], overburden pressure gradient [green], sampled pore pressure gradient [red], raw pore pressure gradient [gray]. (e) Pressure plots: Hydrostatic pressure [blue], pore pressure [red], raw pore pressure [gray], lithostatic pressure [green]

.

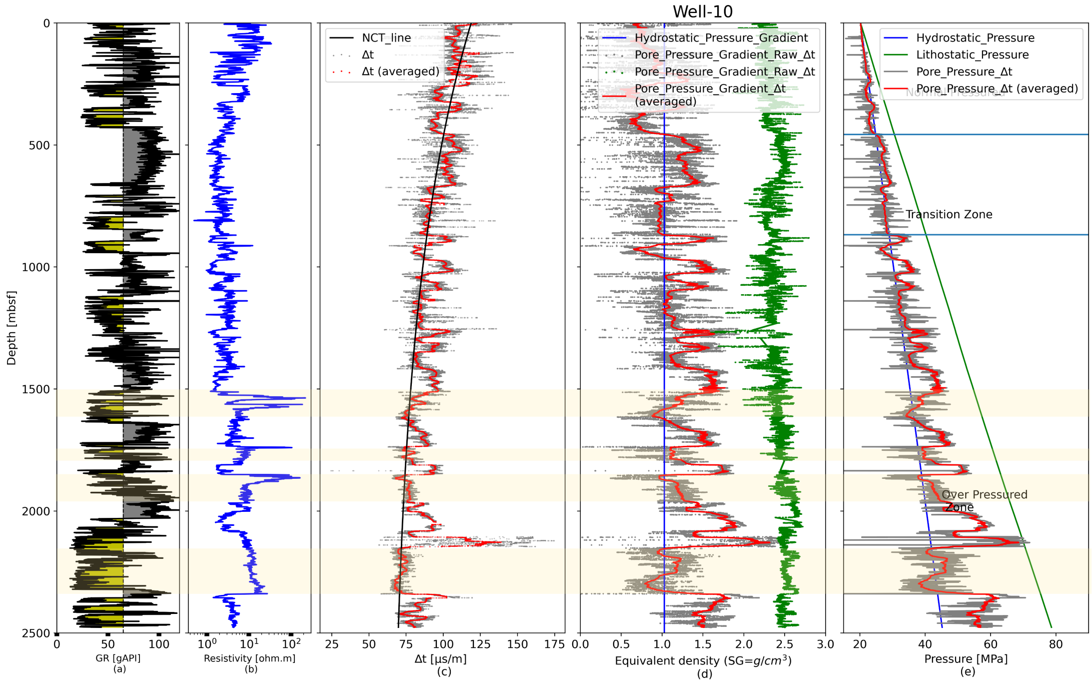

Figure 4. Pore pressure prediction from Eaton modelling based on Δt sonic method (a) Logging units (b) Deep electrical resistivity log in $\Omega \cdot$ m (c)Eaton Δt coefficient profile (raw Δt [gray] and sampled Δt [in red]) and NCT line [in black]. (d) Gradient plots: Pressure gradient pressure gradients, the hydrostatic pressure gradient [blue], overburden pressure gradient [green], sampled pore pressure gradient [red], raw pore pressure gradient [gray]. (e) Pressure plots: Hydrostatic pressure [blue], pore pressure [red], raw pore pressure [gray], lithostatic pressure [green]

high resistivity signature values (Figure 4b) are hydrostatically pressured or underpressured (Figure 4 e). The excess pore pressure above the hydrostatic pressure ranges between $P^* \approx 1.33 - 25.75$ MPa, while, the lithostatic load and modified excess pore pressure ranges between ($\lambda \approx 0.51 - 0.97$) and ($\lambda^* \approx 0.2 - 0.9$) respectively.

4.1.3 Pore Pressure Along Well-12

Transit time (Δt) follows the NCT (Figure 5c) between the depth range of 0 to 806 mbsf. Generally, the pore pressure gradient is about 1.0 g/cm^3 (Figure 5d) in this interval. Therefore, the pore pressure is equal to the hydrostatic pore pressure (Figure 5e). Hence, it is considered to be normally pressure or hydrostatically pressure.

Trend deviations are observed between 806 mbsf to 1220 mbsf with pore pressure gradient rising to about 1.42 g/cm^3 (Figure 4d). At this depth the formations are already getting pressurized with increasing pore fluid pressure values higher than the hydrostatic pore pressure (Figure 4e). The excess pore pressure above the hydrostatic pressure ranges between $P^* \approx 1.49 - 3.48$ MPa, while, the lithostatic load and modified excess pore pressure ranges between ($\lambda \approx 0.6-0.8$) and ($\lambda^* \approx 0.19-0.46$) respectively. This interval is considered to be the transitional pore pressure zone.

The bottom of the transitional zone marks the top of the geopressured interval (Figure 5e). Varying trend deviation is consistently observed from the top of the geopressured zone to the bottom of the well (Figure 5 c). In general, the pore pressure gradient rises to a maximum value of 2.1 g/cm^3 (Figure 5d) and alternates back to 1.0 g/cm^3 and to lower values at the bottom of the well. In this interval, the pore pressure consistently increases to values higher than the hydrostatic pressure (Figure 5e). Pore pressure values rises to a maximum value of 65.38 MPa (Figure 5e) but at the bottom of the borehole, intervals with high resistivity signature values (Figure 5b) are hydrostatically pressured or underpressured (Figure 5 e). The excess pore pressure above the hydrostatic pressure ranges between P^* $\approx 1.06 - 24.75$ MPa, while, the lithostatic load and modified excess pore pressure ranges between ($\lambda \approx 0.46 - 0.94$) and ($\lambda^* \approx 0.2 - 0.84$) respectively.

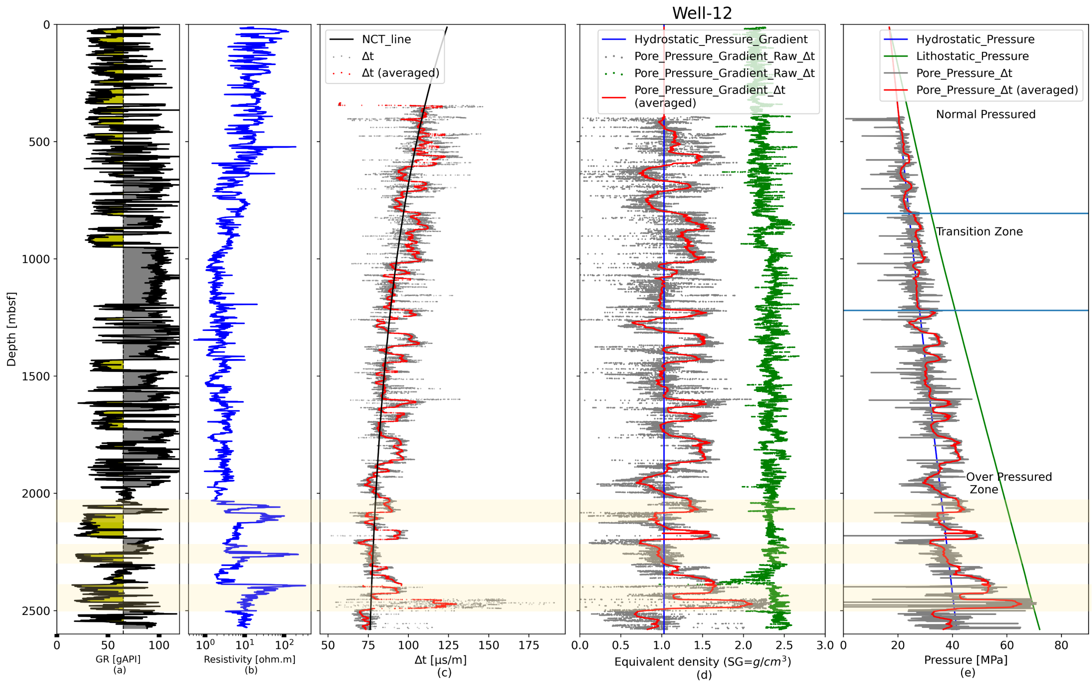

Figure 5. Pore pressure prediction from Eaton modelling based on Δt sonic method (a) Logging units (b) Deep electrical resistivity log in $\Omega \cdot$ m (c)Eaton Δt coefficient profile (raw Δt [gray] and sampled Δt [in red]) and NCT line [in black]. (d) Gradient plots: Pressure gradient pressure gradients, the hydrostatic pressure gradient [blue], overburden pressure gradient [green], sampled pore pressure gradient [red], raw pore pressure gradient [gray]. (e) Pressure plots: Hydrostatic pressure [blue], pore pressure [red], raw pore pressure [gray], lithostatic pressure [green]

.

5 Discussion

5.1 Pore Pressure and Generation Mechanism in Niger Delta

Evidence of the spatial variation of pore pressure in the Niger Delta has been shown using the Eaton's equation in this research. The result of the Eaton's method along the three wells shows similar variability of fluid pressure increase. Even though the top of the geopressured interval varied along the three wells, with Well-05 at 1110 mbsf (3038.28 mbRT or 9968.11 ft below rotary table), Well-10 at 868 mbsf (2873 mbRT or 9425.853 ft below rotary table) and Well-12 at 1220 mbsf (2879 mbRT or 9445.54 ft below rotary table). The bottom of the wells is overly pressured, with Wells 10 and 12 more pressurized than Well-05.

High pore pressure peaks are related to the shale intervals in Figures 3, 4, & 5. This links the generation of high pore pressure in the Offshore Niger Delta with undercompacted sediments. Figure 7 shows a linear relationship between sonic velocity and bulk density. According to Swarbrick (2012); Lahann et al. (2001), such relationship is related to overpressure mecahnism caused by disequilibrium compaction of sediments. Therefore, as observed from Figure 7, the high pore pressure generation mechanism in the Offshore Niger Delta is also related to disequilibrium compaction of sediments.

In Figure 7a & b, it can be observed that there is a slight excursion from the normal trend, without varying density and low effective stress values (Figure 7ai, aii, bi & bii). This excursion from normal trend suggest that another mechanism is responsible for the generation of high pore pressure according to Swarbrick (2012); Lahann et al. (2001). This mechanism is related to fluid expansion (unloading) and clay diagenesis at the bottom of the well.

The predicted pore pressure values obtained in this research depict the over-pressurization state of the Niger Delta. This stems from the fact that the NCT was properly estimated in the three wells. The exponent value used for this work is m = 3, which is applicable in tertiary basins such as the Niger Delta and basins in which the over-pressure state is predominantly caused by disequilibrium compaction (A. Mouchet & Mitchell, 1989).

Note that the value, m = 3 is rarely used in the Niger Delta to study high pore pressure. Previous studies in the Onshore Niger Delta (Nwozor et al., 2012; Chukwuma et al., 2013; Asedegbega et al., 2018), have used high values of the Eaton exponent (m= 4.8 - 6.5) to estimate the NCT. Thus suggesting that the main generating mechanism of high pore pressure is by fluid expansion in the Onshore Niger Delta (A. Mouchet & Mitchell, 1989; M. Tingay et al., 2000; M. R. Tingay et al., 2009). However, in this research shows that the main generating mechanism of high pore pressure in the Offshore Niger Delta is by disequilibrium compaction with m=3.

In order to understand the impact of the Eaton exponent variation in the Offshore Niger Delta, we conducted a parametric study using Equation 6 by varying the values of m = 3 - 6. Our results (Figure 6) show that high pore pressure at the bottom of the wells, rises close to lithostatic pressure and in some intervals in Well-10 & well-12 it is above the lithostatic pressure. At the bottom of the well-05 the pore pressure derived from exponent m=5-6 is higher than the fracture gradient. Therefore, this can initiate rock deformation leading to borehole collapse and blowout condition during drilling. Adopting higher values of the Eaton exponent will provide inaccurate pore pressure values in the Offshore Niger Delta.

On the other-hand, if the observations of Nwozor et al. (2012); Chukwuma et al. (2013); Asedegbega et al. (2018) are reasonable, then different generating mechanisms are responsible for high pore pressure values in the Niger Delta at a regional scale. The generating mechanism in the Onshore and Offshore delta are primarily by unloading and disequilibrium compaction respectively.

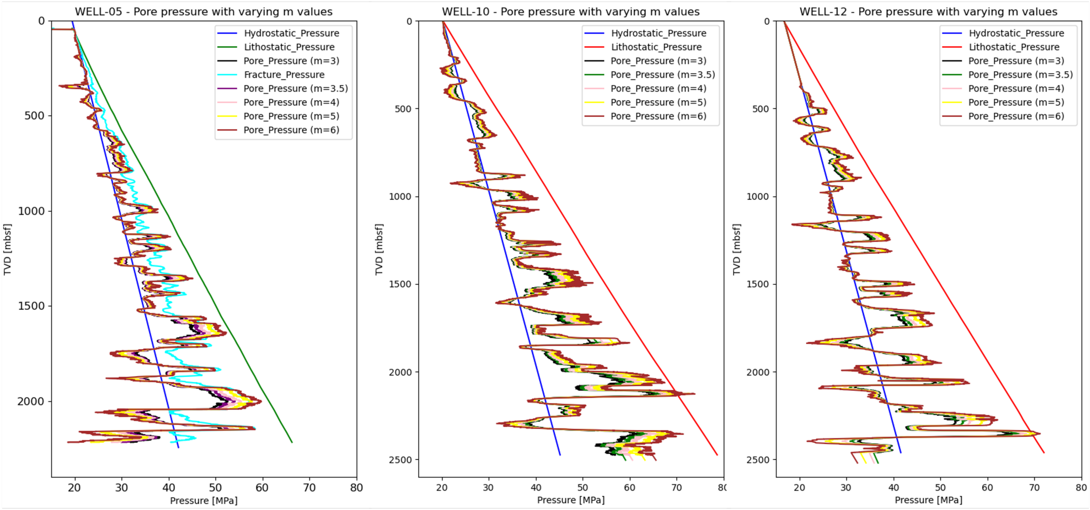

Figure 6. Pore pressure prediction from Eaton modelling based on Δt sonic method with varying values of m=3, m=3.5, m=4, m=5, m=6 across the three wells.

Finally, our work has shown that the several mechanisms are responsible for the overpressurization state in offshore Niger Delta: Primarily by disequilibrium compaction and other factors such as unloading (fluid expansion), shale diagenesis, and structural influence.

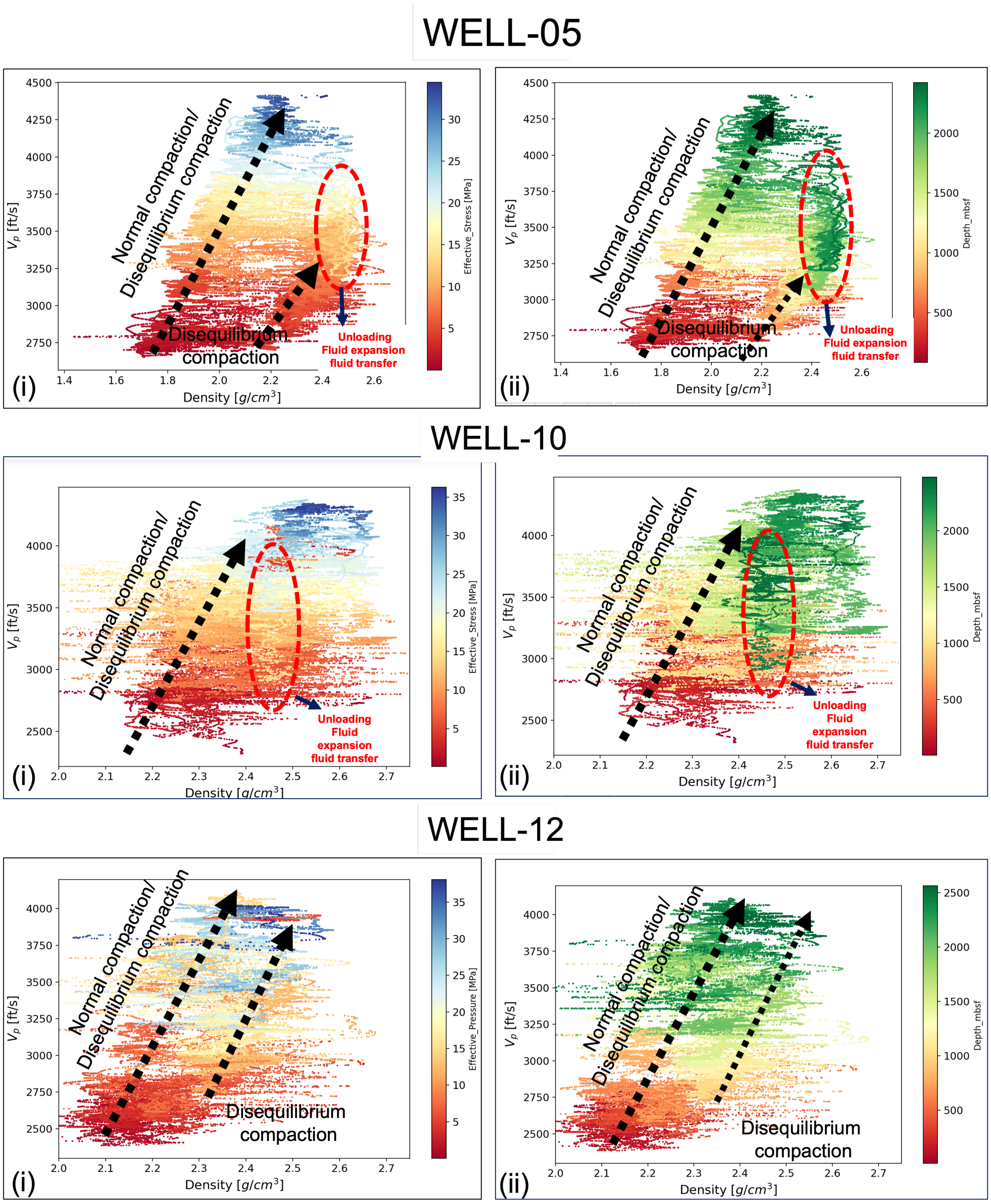

Figure 7. Cross-plots of sonic velocity-density along the three wells (a, b, c) coloured data points with effective pressure (MPa) in ai, bi, ci and measured depth (mbsf) in aii, bii and cii.

5.2 Implication on Reservoir quality and Drilling Activities

High resistivity signatures on Figures 3b, 4b and 5b are potential hydrocarbon bearing reservoir intervals. It is observed that within these intervals, the pore pressure drops to hydrostatic pressure. Low pressures below hydrostatic can also be observed at the bottom of the wells, hence, a typical signature of a depleted hydrocarbon reservoir. These might be related to the poor sealing capacity of both the shales and structural features. Extensive work and correlation with other datasets is needed to confirm this assumption.

The pore pressure gradients across the the three wells guides the choice of mud weight used for drilling future wells in this field. Based on the variable onset of pore pressure in the Offshore Niger Delta, the recommended mud pressure should be slightly higher than the pore pressure in order to maintain pressure balance between wellbore mud pressure and formation pressure. As discussed by Pwavodi and Doan (2022), we recommend that downhole annular mud pressure sensors should be attached to the bottom hole assembly to provide realtime mud pressure while drilling.

6 Conclusion

In this article we predicted the spatial distribution of pore pressure in offshore Niger Delta by processing the well logs using python programming language. Our results have shown the evidence of overpressures with values increasing from the depth of 1110 mbsf (3038.28 mbRT or 9968.11 ft below rotary table) in Well-05, 868 mbsf (2873 mbRT or 9425.853 ft below rotary table) at Well-10 and 1220 mbsf (2879 mbRT or 9445.54 ft below rotary table) in Well-12. Pore pressure onsets is within the Agbada Formation and it is expected to increase to higher values in the Akata shales at deeper depths. In the paralic Agbada Formation the excess pore pressure ratios above hydrostatic pressure varies averagely in the three wells between $P^* = 1.06 - 12.96$ MPa, $P^* = 1.33 - 25.75$ MPa, $P^* = 1.06 - 24.75$ MPa in Well-05, Well-10, & Well-12 respectively. While the lithostatic load in Well-05 is $\lambda = 0.63 - 0.87$ & $\lambda^* = 0.1 - 0.59$; in Well-10 is $\lambda = 0.46 - 0.94$ & $\lambda^* = 0.2 - 0.84$; and in Well-12 is $\lambda = 0.51 - 0.97$ & $\lambda^* = 0.2 - 0.9$.

Our results have provided a more accurate representation of the normal compaction trend in the Offshore Niger Delta, hence providing a reasonable state of the consolidation history of the sediments. We have shown that the use of Eaton's exponent in different parts of the Niger Delta needs to be applied with caution in order to properly depict the regional consolidation of the sediments. It has also been shown that the pore pressure generation mechanisms in the Offshore Niger Delta is by disequilibrium compaction, unloading and shale diagenesis.

We recommend that strong integration is needed with core samples and numerical models for proper modelling of the consolidation history and pore pressure distribution at a regional scale in the Niger Delta Basin.

Data Availability Statement

The input files, loading and python modules are accessible at the Zenodo data repository: https://doi.org/10.5281/zenodo.7013968

References

Abijah, F. A., & Tse, A. C. (2016). Geomechanical evaluation of an onshore oil field in the niger delta, nigeria. *IOSR Journal of Applied Geology and Geophysics*, *4*, 99-111. Retrieved from `www.iosrjournals.org` doi: 10.9790/0990-041199111

Adewole, E. O., Macdonald, D. I., & Healy, D. (2016, 11). Estimating density and vertical stress magnitudes using hydrocarbon exploration data in the onshore northern niger delta basin, nigeria: Implication for overpressure prediction. *Journal of African Earth Sciences*, *123*, 294-308. doi: 10.1016/j.jafrearsci.2016.07.009

Alabere, A. O., & Akangbe, O. K. (2021, 10). Pore pressure prediction in niger delta high pressure, high temperature (hp/ht) domains using well logs and 3d seismic data: a case study of x-field, onshore niger delta. *Journal of Petroleum Exploration and Production Technology*, *11*, 3747-3758. doi: 10.1007/s13202-021-01264-5

A. Mouchet, J., & Mitchell. (1989). *Abnormal pressures while drilling.*

Asedegbega, J. E., Oladunjoye, M. A., & Nwozor, K. K. (2018, 6). A method to reduce the uncertainty of pressure prediction in hpht prospects: a case study of onshore niger delta depobelt, nigeria. *Journal of Petroleum Exploration and Production Technology*, *8*, 375-380. doi: 10.1007/s13202-017-0401-8

Avbovbo, A. (1978). Geologic notes tertiary lithostratigraphy of niger delta'. *The American Association of Petroleum Geologists Bulletin*, *62*(2), 295-306. Retrieved from `https://pubs.geoscienceworld.org/aapgbull/article-pdf/62/2/295/4454368/aapg_1978_0062_0002_0295.pdf`

Baouche, R., Sen, S., Sadaoui, M., Boutaleb, K., & Ganguli, S. S. (2020). Characterization of pore pressure, fracture pressure, shear failure and its implications for drilling, wellbore stability and completion design – a case study from the takouazet field, illizi basin, algeria. *Marine and Petroleum Geology*, *120*, 104510. Retrieved from `https://www.sciencedirect.com/science/article/pii/S0264817220302932` doi: https://doi.org/10.1016/j.marpetgeo.2020.104510

Chukwuma, M., Brunel, C., Cornu, T., & Carre, G. (2013). Open access case report overcoming pressure limitations in niger delta basin: "digging deep into new frontier on block-x". *J Geol Geosci*, *2*, 1. doi: 10.4172/2381-8719.1000112

Davis, D., Suppe, J., & Dahlen, F. A. (1983). Mechanics of fold-and- thrust belts and accretionary wedges. *Journal of Geophysical Research*, *88*(B2), 1153–1172. doi: 10.1029/JB088iB02p01153

Dosunmu, U. N. A. (2002). Analysis of pore pressure using geophysical methods. *Global Journal of Engineering Research*, *3*, 39-46.

Doust H, O. E. (1990). Niger Delta, In: Edwards, J. D. and Santogrossi, P. A.(eds) Divergent/Passive Margin Basins. *American Association of Petroleum Geologists*, *48*, 201-238.

Eaton, B. A. (1972). The effect of overburden stress on geopressure prediction from well logs. *Journal of Petroleum Technology*, *24*(08), 929–934. doi: 10.2118/3719-pa

Eaton, B. A. (1975). *The equation for geopressure prediction from well logs.* (SPE-5544-MS) doi: 10.2118/5544-MS

Ebong, E. D., Akpan, A. E., & Ekwok, S. E. (2020, 2). Stochastic modelling of spatial variability of petrophysical properties in parts of the niger delta basin, southern nigeria. *Journal of Petroleum Exploration and Production Technology*, *10*, 569-585. doi: 10.1007/s13202-019-00787-2

Ejedawe, J. (1989). The eastern niger delta: geological evolution and hydrocarbon occurrences. *SPDC Internal Report,Exploration Note*, *2*, 12-23.

Ejedawe, J., Coker, S., D.O., L.-A., Alofe, K., & Adoh, F. (1984). Evolution of oil-generative window and oil and gas occurrence in tertiary niger delta basin. *American Association of Petroleum Geologists Bulletin*, *68*, 1744-1751.

Emudianughe, J., & Ogagarue, D. (2019). Well-based pore pressure validation: A case study of akos field, coastal depobelt, niger delta basin. *FUPRE Journal of Scientific and Industrial Research*, *3*. Retrieved from `https://pubs.usgs.gov/of/1999/ofr-99-`

Evamy, B. D., Haremboure, J., Kamerling, P., Knaap, W. A., Molloy, F. A., & Rowlands, *P. H.* (1978). *Hydrocarbon habitat of tertiary niger delta* (Vol. 62).

Ganguli, S. S., & Sen, S. (2020). Investigation of present-day in-situ stresses and pore pressure in the south cambay basin, western india: Implications for drilling, reservoir development and fault reactivation. *Marine and Petroleum Geology*, *118*, 104422. Retrieved from `https://www.sciencedirect.com/science/article/pii/S0264817220302051` doi: https://doi.org/10.1016/j.marpetgeo.2020.104422

Gercek, H. (2007). Poisson's ratio values for rocks. *International Journal of Rock Mechanics and Mining Sciences*, *44*(1), 1–13.

Haack, R. C., Sundararaman, P., Diedjomahor, J. O., Xiao, H., Gant, N. J., May, E. D., & Kelsch, K. (2000, 01). Niger Delta Petroleum Systems, Nigeria. In *Petroleum Systems of South Atlantic Margins.* American Association of Petroleum Geologists. Retrieved from `https://doi.org/10.1306/M73705C16` doi: 10.1306/M73705C16

Holand, P. (2001). *Deepwater kicks and bop performance : unrestricted version* (Vol. STF38 A01419). Trondheim: SINTEF, Industrial Management, Safety and Reliability.

Hubbert, M. K., Aime, M., Willis, D. G., & Aime, J. M. (1957). *Mechanics of hydraulic fracturing.*

Ichara, M., & Avbovbo, A. (1985). How to handle abnormal pressures in nigeria's niger delta area. *Oil Gas Journal.*, *83:10*. Retrieved from `https://www.osti.gov/biblio/5103188`

Imhanzuaria, D., & Bello, K. (2019). Evaluation of poisson's ratio range for fracture pressure gradient (fpg) prediction for niger delta formation. *Nigerian Journal of Technology*, *38*(3), 628–635.

Knox, G., & Omatsola, E. (1989). Development of the cenozoic niger delta in terms of the "escalator regression" model and impact on hydrocarbon distribution. *Proceedings KNGMG Symposium "Coastal Lowlands, Geology and Geotechnology*, 181-202.

Lahann, R., Lahann, W., McCarty, D., & Hsieh, J. (2001). *Influence of clay diagenesis on shale velocities and fluid-pressure.* Retrieved from `https://www.wizdom.ai/publication/10.4043/13046-MS/title/influence_of_clay_diagenesis_on_shale_velocities_and_fluid_pressure` doi: 10.4043/13046-MS

Michele L. Tuttle, R. R. C., & Brownfield, M. E. (1999). *The niger delta petroleum system; niger delta province, nigeria, cameroon, and equatorial guinea, africa.* U.S. Geological Survey. doi: https://doi.org/10.3133/ofr9950H

Nwankwo, C. N., & Kalu, S. O. (2016). Integrated approach to pore pressure and fracture pressure prediction using well logs: Case study of onshore niger-delta sedimentary basin. *Open Journal of Geology*, *06*, 1279-1295. doi: 10.4236/ojg.2016.610094

Nwaufa W.A., O. C., Horsfall D.E. (2006). *Advances in deep drilling in the niger delta, 1970-2000 : Nigerian agip oil company (naoc) experience* (Vol. 62) (No. 2).

Nwozor, K., Ozumba, B. M., & Belushi, C. J. E. (2012). *A relationship between diagenetic clay minerals and pore pressures in an onshore niger delta field plausible model for predicting abnormal pressure in hpht wells in the eocene depobelt, onshore niger delta basin, nigeria view project petrographic and palynological analyses of the eze-aku group in akpoha and environs, southern benue trough, nigeria view project.* Retrieved from `https://www.researchgate.net/publication/317179408`

Omoboriowo, A. O., & Chiadikobi, K. C. (2012). Depositional environment and petrophysical characteristics of "lepa" reservoir, amma field, eastern niger delta, nigeria..

Opara, A., Onuoha, K., Anowai, C., Mbah, R., & Onu, N. (2009). *Overpressure and trap integrity studies in parts of the niger delta basin: Implications for hydrocarbon prospectivity.* Retrieved from `https://www.researchgate.net/publication/272563965`

Opara, A., Onuoha, K. M., Anowai, C., Onu, N. N., & Mbah, R. O. (2013, 3). Pressions de pores et prévisions de l'intégrité des couvertures à partir de données sismiques 3d: Le cas du grand sous-bassin d'ughelli, delta du niger. *Oil and Gas Science and Technology*, *68*, 383-396. doi: 10.2516/ogst/2011157

Owoyemi, A. O., & Willis, B. J. (2006). Depositional patterns across syndepositional normal faults, niger delta, nigeria. *Journal of Sedimentary Research*, *76*, 346-363.

Pwavodi, J., & Doan, M.-L. (2022). Direct evidence of high pore pressure at the toe of the nankai accretionary prism. *Earth and Space Science Open Archive*, 40. Retrieved from `https://doi.org/10.1002/essoar.10510789.1` doi: 10.1002/essoar.10510789.1

Reijers, T., Petters, S., & Nwajide, C. (1997). Chapter 7 the niger delta basin. In R. Selley (Ed.), *African basins* (Vol. 3, p. 151-172). Elsevier. Retrieved from `https://www.sciencedirect.com/science/article/pii/S187459979780010X` doi: https://doi.org/10.1016/S1874-5997(97)80010-X

Rubey, W. W., & King Hubbert, M. (1959). Role of fluid pressure in mechanics of overthrust faulting: II. Overthrust belt in geosynclinal area of western Wyoming in light of fluid-pressure hypothesis. *Bulletin of the Geological Society of America*, *70*(2), 167–206. doi: 10.1130/0016-7606(1959)70[167:ROFPIM]2.0.CO;2

Short, K., & Stauble, A. (1967). Outline of the geology of niger delta. *American Association of Petroleum Geologists Bulletin*, *51*, 761-779.

Skalle, P., & Podio, A. L. (1998). Trends extracted from 1,200 Gulf coast blowouts during 1960-1996. *World Oil*, *219*(6), 67–72.

Swarbrick, R. (2012). Review of pore-pressure prediction challenges in high-temperature areas. *The Leading Edge*, *1288-1294*. doi: doi:10.1190/tle31111288.1

Terzaghi, K., & Peck, R. B. (1948). *Soil Mechanics in Engineering Practice* (1st ed.). John wiley & sons.

Terzaghi, K., Peck, R. B., & Mesri, G. (1968). *Soil Mechanics in Engineering Practice* (3rd ed.). Wiley.

Tingay, M., Hillis, R., Swarbrick, R., Mildren, S., Morley, C., & Okpere, E. (2000). The sonic and density log expression of overpressure in brunei darussalam. In *Overpressure 2000–workshop proceedings: Cd volume, paper op2000_21.*

Tingay, M. R., Hillis, R. R., Swarbrick, R. E., Morley, C. K., & Damit, A. R. (2009). Origin of overpressure and pore-pressure prediction in the baram province, brunei. *American Association of Petroleum Geologists Bulletin*, *93*, 51-74. doi: 10.1306/08080808016

Tobin, H., & Kinoshita, M. (2007). The IODP Nankai trough seismogenic zone experiment. *Scientific Drilling*, *5*(1 SUPPL. 1), 39–41. doi: 10.2204/iodp.sd.s01.30.2007

Tuttle, M. L., Charpentier, R. R., & Brownfield, M. E. (1999). *The niger delta petroleum system: Niger delta province, nigeria, cameroon, and equatorial guinea, africa.* US Department of the Interior, US Geological Survey.

Udo, K. I., George, ., Akankpo, ., Azuoku, ., & Aka, M. . U. (2020). *International journal of advanced geosciences determining fracture pressure gradients from well logs* (Vol. 8). Retrieved from `www.sciencepubco.com/index.php/IJAG`

Ugwu, S. A., & Nwankwo, C. N. (2014, 9). Integrated approach to geopressure detection in the x-field, onshore niger delta. *Journal of Petroleum Exploration and Production Technology*, *4*, 215-231. doi: 10.1007/s13202-013-0088-4

Weber, K., & Daukoru, E. (1975). Petroleum Geology of the Niger Delta. *Proceedings of the Ninth World Petroleum Congress*, *8*(2), 210–221.

Whiteman, A. (1982). *Nigeria: Its petroleum geology, resources and potential* (Vol. 1). Springer Dordrecht. doi: https://doi.org/10.1007/978-94-009-7361-9

Yaolin Shi, & Chi-Yuen Wang. (1988). Generation of high pore pressures in accretionary prisms: inferences from the Barbados Subduction Complex. *Journal of Geophysical Research*, *93*(B8), 8893–8910.

Zhang, J. (2011). Pore pressure prediction from well logs: Methods, modifications, and new approaches. *Earth-Science Reviews*, *108*, 50–63. doi: 10.1016/j.earscirev.2011.06.001

Zhang, J., & Yin, S. (2017). Real-time pore pressure detection: Indicators and improved methods. *Geofluids*(1). doi: 10.1155/2017/3179617

Zhang, J. J. (2019). *Abnormal pore pressure mechanisms.* doi: 10.1016/b978-0-12-814814-3.00007-1